Condensation energy of a spin-1/2 strongly interacting Fermi gas

N. Navon,[1,*] S. Nascimbène,[1] X. Leyronas,[2,†] F. Chevy,[1] and C. Salomon[1]

[1]*Laboratoire Kastler Brossel, CNRS, UPMC, Ecole Normale Supérieure, 24 rue Lhomond, 75231 Paris, France*

[2]*Laboratoire de Physique Statistique, Ecole Normale Supérieure, UPMC Université Paris 06, Université Paris Diderot, CNRS, 24 rue Lhomond, 75005 Paris, France*

(Received 4 April 2013; revised manuscript received 15 October 2013; published 6 December 2013)

We report a measurement of the condensation energy of a two-component Fermi gas with tunable interactions. From the equation of state of the gas, we infer the properties of the normal phase in the zero-temperature limit. By comparing the pressure of the normal phase at $T = 0$ to that of the low-temperature superfluid phase, we deduce the *condensation energy*, i.e., the energy gain of the system upon being in the superfluid rather than the normal state. We compare our measurements to a ladder approximation description of the normal phase and to a fixed-node Monte Carlo approach, finding excellent agreement. We discuss the relationship between condensation energy and pairing gap in the BEC-BCS crossover.

DOI: 10.1103/PhysRevA.88.063614 PACS number(s): 03.75.Ss, 05.30.Fk, 34.50.−s

I. INTRODUCTION

From a thermodynamic point of view, a superconducting state is favored compared to a normal state when the free energy of the former (E_S) is lower than that of the latter (E_N). This energy difference, called the *condensation energy*, is a central concept in the BCS theory of conventional superconductivity. For example, in the weakly interacting regime the condensation energy is related to the superfluid pairing gap Δ by

$$E_c = E_N - E_S = N_f \frac{\Delta^2}{2}, \tag{1}$$

where N_f is the density of states at the Fermi energy [1]. For superconductors, the condensation energy is obtained from the measurement of the critical magnetic field H_c at which superconductivity is quenched,

$$E_c = \mu_0 \frac{H_c^2}{2}, \tag{2}$$

where μ_0 is the vacuum magnetic permeability [1]. While BCS theory [and relation (1)] have proven very successful to explain conventional superconductivity, a similar description to explain exotic forms of superconductivity, such as encountered in cuprate or iron-compound materials, is still lacking. In particular, the role of the condensation energy in high-T_c superconductors is thought to give insight into the mechanism that could be responsible for driving the superconducting transition (see, e.g., [2–5], and references therein), though its extraction from experimental data or even its relevance is still a hotly debated issue [6–8].

Ultracold atoms are now increasingly used as test beds to experimentally explore quantum many-body physics, owing to their high degree of control [9]. It has become possible to simulate Hamiltonians from various fields of physics, such as neutron matter or condensed matter physics in simple systems. Moreover, interactions between ultracold atoms, characterized by the s-wave scattering length a, can be tuned via magnetic Feshbach resonances, giving access to the regime of strong interactions.

In this article, we investigate the condensation energy of a dilute spin-1/2 strongly interacting Fermi gas with a variable interaction strength. We show that the condensation energy can be measured by applying a chemical potential imbalance between the two spin states which is the analog of a magnetic field in superconductors. In contrast to superconductors, we explore a regime where the effective Zeeman energy is of the order of the Fermi energy. We compare our experimental results to a diagrammatic theory, finding excellent agreement.

II. NORMAL-STATE PRESSURE

The experimental setup was presented in [13]. Our system is a quantum gas of ^{6}Li prepared in a mixture of its two lowest energy spin states.

The gas is loaded into a single-beam dipole trap, providing a radial (strong) confinement, while the axial (weak) confinement (z axis) is provided by magnetic coils. This results in a cigar-shaped trap. The interactions are tuned using a pair of coils in the Helmholtz configuration in order to create a large homogeneous bias field to tune the scattering length a via the 832.18-G Feshbach resonance [10]. The mixture is cooled to quantum degeneracy by lowering the trap depth, and absorption images perpendicular to the weak direction are recorded to obtain the *in situ* density distributions along the z axis. Previous theoretical [11,12] and experimental [13,14] studies have demonstrated that the density profiles of a trapped spin-imbalanced Fermi gas can be used to extract the equation of state (EoS) of the corresponding homogeneous system via the pressure formula, $P(\mu_1,\mu_2,T) = \frac{m\omega_r^2}{2\pi}[\bar{n}_1(z) + \bar{n}_2(z)]$, where ω_r is the radial trapping frequency, and $\bar{n}_i(z) = \int d^2r\, n_i(r,z)$ is the doubly integrated density distribution of spin species i ($i = 1,2$).

At unitarity, where the scattering length a diverges, we previously measured the pressure of the spin-balanced gas as a function of the reduced temperature $t = k_B T/\mu$ (where $2\mu = \mu_1 + \mu_2$) [13], as well as the pressure of the spin-imbalanced

*Present address: Cavendish Laboratory, University of Cambridge, J. J. Thomson Avenue, Cambridge CB3 0HE, United Kingdom; nn270@cam.ac.uk

†leyronas@lps.ens.fr

gas at $t \approx 0$ as a function of the spin-polarizing field $b = \frac{\mu_1-\mu_2}{\mu_1+\mu_2}$. We suggested that the low-temperature properties of the normal phase of the Fermi gas were consistent with a Fermi-liquid behavior [19]. As a result, the low-temperature and low-imbalance limit of the pressure of the unitary gas can be written as

$$h(t,b) = \frac{P(\mu_1,\mu_2,T)}{2P_0(\mu)} \simeq \xi_N^{-3/2} + \frac{\tilde{\chi} b^2}{2} + \frac{\tilde{c}_V t^2}{2}, \qquad (3)$$

where $P_0(\mu) = \frac{1}{15\pi^2}(\frac{2m}{\hbar^2})^{3/2}\mu^{5/2}$ is the ideal Fermi-gas pressure. The response coefficient to temperature t is the dimensionless specific heat $\tilde{c}_V$, while the response to the polarizing field b is the dimensionless magnetic susceptibility $\tilde{\chi}$ (equal to $5\pi^2/8$ and $15/4$, respectively, for the ideal Fermi gas). The magnetic susceptibility has been the subject of a previous work [18], and we focus here on the measurement of the pressure of the normal phase $\xi_N^{-3/2}$ in the $t = 0$ and $b = 0$ limits. In the (t,b) plane, our measurements of the EoS of the unitary gas have been performed along two directions: the unpolarized gas as a function of temperature $h(t,b = 0)$ (Fig. 1) and the low-temperature polarized gas versus the chemical potential imbalance $h(t = 0,b)$ [Fig. 2(a)]. The quadratic behavior of the pressure versus both b and t supports the Fermi-liquid interpretation of the low-temperature thermodynamic properties of the normal phase. However, the system will ultimately undergo a second-order phase transition to a superfluid state, and below the temperature $t_c \sim 0.33$, the pressure of the spin-balanced gas deviates from the t^2 behavior. In contrast, at $t = 0$, the spin-imbalanced gas ($\mu_1 \neq \mu_2$) undergoes a first-order phase transition to an unpolarized superfluid phase when $h_S(0,0) = h_N(0,0) + \tilde{\chi} b^2/2$. This condition is the analog of Eq. (2), and at unitarity it yields the critical chemical potential imbalance $b_c \approx \sqrt{0.8}$ [see Fig. 2(a)]. This is demonstrated by the discontinuity in the slope of h vs b^2. From Eq. (3), and extrapolating the Fermi-liquid behavior to the zero-temperature and spin-balanced limits, we measure the $T = 0$ dimensionless pressure of the spin-balanced unitary gas in the normal phase $\xi_N^{-3/2}$. In the first limit ($t \to 0, b = 0$) we find $\xi_N = 0.48(2)$, while in the second one ($t = 0, b \to 0$), we extract $\xi_N = 0.53(2)$ [see (red) X's in Figs. 1 and 2(a)]. The proximity of these values, taken for two very different limiting regimes, is remarkable and further supports the accurate

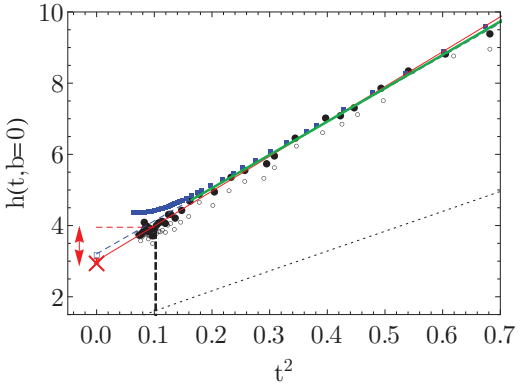

FIG. 1. (Color online) Reduced pressure $h(t,b) = P(\mu_1,\mu_2,T)/2P_0(\bar{\mu})$ of the spin-1/2 unitary Fermi gas, where P_0 is the $T = 0$ Fermi pressure of an ideal gas, t the reduced temperature k_BT/μ, and $b = 0$ the unpolarized gas. Open black circles are data from [13] taken at $B = 834$ G, while filled black circles include a small correction due to a recently determined downshift of the Feshbach resonance [10]. This correction is estimated using Tan's contact calculated by the bold diagrammatic Monte Carlo (bDMC [16]) (see Appendix B for details). The Fermi-liquid fit is shown as the solid red line, and the extrapolated zero-temperature pressure of the normal state $\xi_N^{-3/2}$ is represented by the (red) X. MIT data from [15] are represented by (blue) squares; the corresponding fit, by the dashed (blue) line; and the extrapolation at $t = 0$, by the open (blue) square. The bDMC calculation [16] is shown by the solid green line. The agreement with the bDMC data is excellent, while a small discrepancy from the MIT data is visible near the superfluid-to-normal transition around $t_c = 0.40$ [15] or $t_c = 0.33$ here [17] (the latter represented by the dashed vertical line). The dashed horizontal (red) line corresponds to the superfluid pressure; the dotted black line, to the ideal gas.

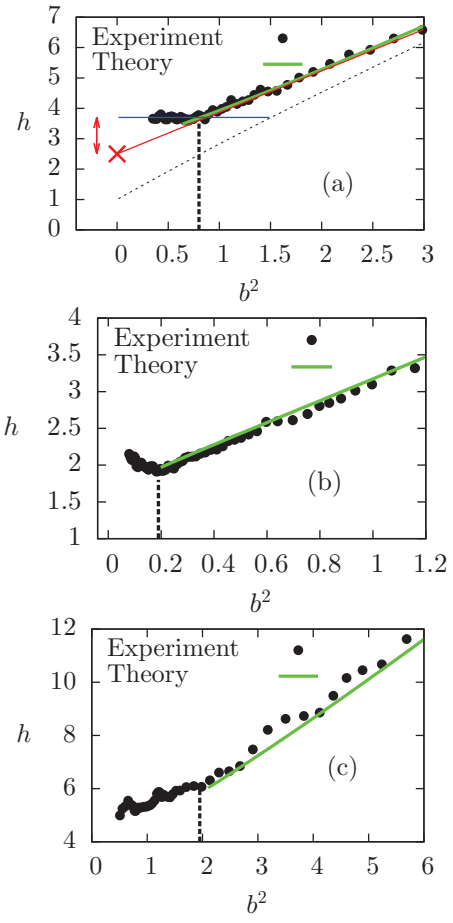

FIG. 2. (Color online) Pressure of the spin-imbalanced gas in the BEC-BCS crossover at $t = 0$. The position of the first-order phase transition to the superfluid is shown by the vertical dashed black line. (a) Unitary limit. The Fermi-liquid fit is shown by the solid red line; the $t = 0$ equation of state in the superfluid phase, by the solid horizontal blue line. The pressure of the noninteracting gas is displayed as the dotted gray line. The $t = 0$ and $b = 0$ extrapolation of the normal phase pressure is shown by the (red) X; the condensation pressure, by the double-arrows. (a–c) Results of the ladder approximation for the normal phase are shown in green for $\delta = 0, -0.58$, and $+0.2$, respectively.

description of the normal phase of the unitary gas as a Fermi liquid. This value is in good agreement with the experimental value, 0.46(1) [15], and close to the values calculated using Monte Carlo methods: 0.54 [19], 0.56, [20], and 0.52 [21].

III. COMPARISON TO THE LADDER APPROXIMATION THEORY

The problem of the zero-temperature balanced superfluid Fermi gas has been the subject of thorough theoretical investigations [22]. However, much less work has been devoted to the EoS of the zero-temperature normal phase [20]. We show below that our experimental results can be quantitatively reproduced using the ladder approximation [23,24]. This theory includes the repeated two-body scattering between particle 1 and particle 2 described by the scattering length a. In particular, for $a^{-1} > 0$, it contains the physics of a molecular state. We use the finite-temperature formalism and take the zero-temperature limit. The self-energy for particles 2, which physically describes the effect of interaction between particles, is given by (we take $\hbar = 1$)

$$\Sigma_2(k,i\omega) = \int \frac{d^3\mathbf{K}}{(2\pi)^3} \int_{i\mathbb{R}} \frac{d\Omega}{2\pi i} \frac{\Gamma(K,\Omega)}{\left[\Omega - i\omega + \mu_1 - \frac{(\mathbf{K}-\mathbf{k})^2}{2m}\right]}, \quad (4)$$

where the two-particle vertex Γ is given by

$$\Gamma(K,\Omega)^{-1} = \frac{m}{4\pi\, a} + \Pi(K,\Omega), \quad (5)$$

where $\Pi(K,\Omega)$ is the pair bubble [24]. At zero temperature, $\Pi(K,\Omega)$ can be calculated analytically. The pairing instability, signaling a second-order phase transition, is found using the Thouless criterion $\Gamma^{-1}(0,0) = 0$. For given μ_1 and a, this happens for a critical value of the chemical potential μ_{2c} of particles 2. In order to stay in the normal phase, we have performed our calculations for $\mu_2 < \mu_{2c}$. The integration on Ω can be performed by deforming the integration contour in the half-plane $\mathrm{Re}(\Omega) < 0$. In this way, we pick the singularities of the integrand in Eq. (4) and get three contributions corresponding to the pole of $(\Omega - i\omega + \mu_1 - \frac{(\mathbf{K}-\mathbf{k})^2}{2m})^{-1}$ (Σ_L), the branch cut of $\Gamma(K,\Omega)$ (Σ_Γ), and the molecular pole $\Omega_0(K)$ (for $a^{-1} > 0$) of $\Gamma(K,\Omega)$ (Σ_m) [24]. $\Omega_0(K) + 2\mu$ represents physically the energy of a molecule of momentum $\mathbf{K}$. We find that in the normal phase $\Omega_0(K) > 0$. As a consequence, when we deform the integration contour in $\mathrm{Re}(\Omega) < 0$, we do not get any contribution from the molecular pole of Γ, and therefore we have $\Sigma_m = 0$. This is consistent with the physical argument in favor of the absence of molecules in the normal phase. Indeed, if we had some molecules in the system, they would be condensed at zero temperature. Therefore the system would be superfluid, and we would no longer be entitled to use Eq. (4). We deduce the minority density n_2 using the Fermi-liquid-type relation due to Landau,

$$\mu_2 = \frac{k_{F,2}^2}{2m} + \Sigma_2(k_{F,2},0), \quad (6)$$

where, by definition, $k_{F,2} \equiv (6\pi^2 n_2)^{1/3}$, is the Fermi wave vector of particles of type 2. For given μ_1, μ_2, and a, this is an implicit equation for $k_{F,2}$ and, hence, n_2. Another approach to calculation of the minority density relies on the interpretation of the momentum distribution obtained from the self-energy, Eq. (4). These two methods give very similar results (see Appendix A for details). As found in [25], we find a no zero density n_2 for a chemical potential μ_2 larger than the *polaron* [25,26] chemical potential $\mu_p(\mu_1)$. In practice, we fix $\mu_1 > 0$, then solve Eq. (6) for a given $\mu_2 \geqslant \mu_p(\mu_1)$. The pressure is determined by integrating the density using the Gibbs-Duhem relation,

$$P(\mu_1,\mu_2) = P_0(\mu_1) + \int_{\mu_p}^{\mu_2} d\mu_2' \frac{1}{6\pi^2}[k_{F,2}(\mu_1,\mu_2')]^3. \quad (7)$$

For a fixed μ_1, we calculate the minority density for increasing minority chemical potential between $\mu_p(\mu_1)$ and μ_2. For a sufficiently large chemical potential difference, the system is normal (the pairing susceptibility does not diverge). For sufficiently low b, we calculate the dimensionless EoS $h(\delta,b)$, where δ is the grand-canonical interaction strength, $\delta = \hbar/\sqrt{2m\mu}a$. For all values of $\delta \leqslant 0$, we find a linear behavior of h as a function of b^2. The comparison between experiment and theory is shown for $\delta = 0$ (unitary limit), $\delta = -0.58$ (BCS side of the crossover), and $\delta = 0.2$ (BEC side) in Figs. 2(a), 2(b), and 2(c), respectively. The agreement is very good. However, for increasing $a^{-1} > 0$, the values of b in the normal phase become larger and larger, and as a consequence, the linear fit of h as a function of b^2, valid at low b, is worse. Still, for $\delta = 0.2$ the experimental EoS $h(\delta,b)$ is in good agreement with the ladder approximation calculation above b_c [diagonal (green) line in Fig. 2(c)]. Within the ladder approximation we have determined the critical spin polarizing field b_c at which a pole appears in the vertex function Γ at zero frequency and zero wave vector (Thouless criterion). We found that b_c was always *smaller* than the experimental value of the first-order transition. Our calculation is therefore free of any instability singularity in the normal phase. For the spin susceptibility, we also find a good agreement among the ladder approximation, experiments, and Monte Carlo simulations of [18].

Gathering the results from Fig. 2, we now extract the zero-temperature dimensionless pressure h_N of the normal phase as a function of δ [18]. The resulting EoS of the normal phase $h_N(\delta)$ is plotted in Fig. 3 as open (red) squares together with the ladder approximation calculation [thick lower solid (green) line], showing excellent agreement in the explored crossover. For comparison, the previously measured EoS of the low-temperature gas in the superfluid phase $h_S(\delta)$ is shown as the blue points and upper solid (blue) line fit [14]. The difference between the superfluid and the normal pressure at $T = 0$ thus represents the *condensation pressure*. The superfluid pressure is higher than the normal phase pressure, $h_S(\delta) > h_N(\delta)$, hence the grand potential is lower and the superfluid state is the stable phase at low temperature. Turning to the canonical ensemble the superfluid and normal phase energies ξ_S and ξ_N as a function of the canonical interaction strength $1/k_F a$ can be computed from the pressure measurement in Fig. 3 using a Legendre transform [27]. The measured condensation energy $\xi_N - \xi_S$ is shown as the solid black line in Fig. 4.

IV. COMPARISON TO THE BCS RESULT

In the BCS regime, the condensation energy E_c can be explicitly calculated from the energy of the superconducting and normal states, yielding the well-known result $E_c = \frac{3}{8} N \frac{\Delta^2}{E_F}$,

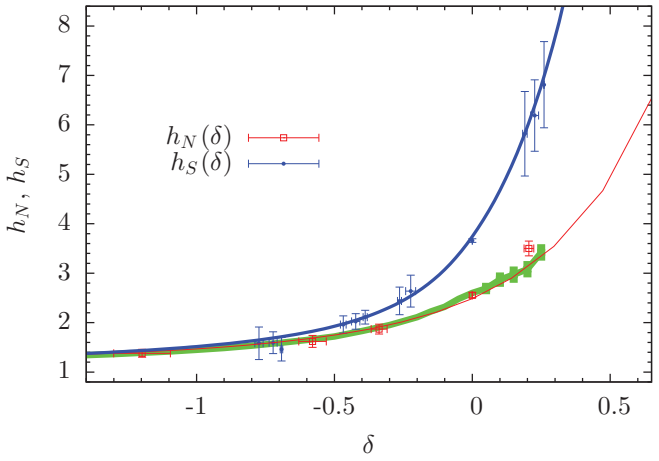

FIG. 3. (Color online) Pressure of the normal h_N [open (red) squares] and superfluid h_S [filled (blue) circles] phases at low temperature in the BEC-BCS crossover measured in [14]. The thick lower solid (green) line is the result of the ladder approximation. The upper solid (blue) line is a guide for the eye, while the lower solid (red) line is the result of fixed-node Monte Carlo calculations [18]. The difference between the blue and the red or green lines is the *condensation pressure*.

where Δ is the single-particle excitation gap, and E_F the Fermi energy. Since $E = \frac{3}{5}NE_F\xi_\alpha(1/k_Fa)$ (where $\alpha = S,N$), the BCS equation becomes

$$\xi_N - \xi_S = \frac{5}{8}\left(\frac{\Delta}{E_F}\right)^2. \tag{8}$$

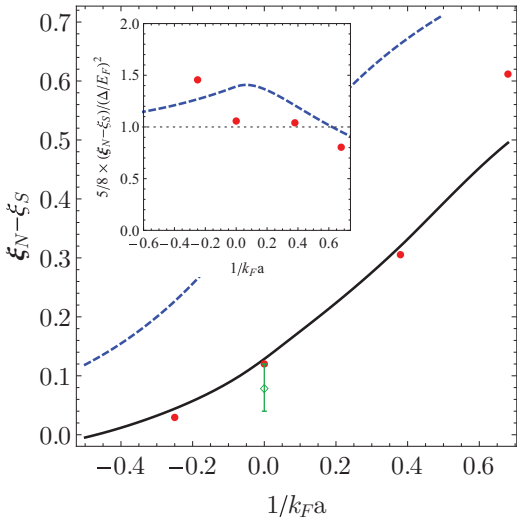

FIG. 4. (Color online) Relation between the condensation energy and the superfluid pairing gap. Dimensionless condensation energy $\xi_N - \xi_S$ versus interaction strength $1/k_Fa$ extracted from the $b \to 0$ extrapolation (solid black line). Filled (red) circles represent the BCS expression, (8), using the values of Δ measured in [28]. The prediction from mean-field BCS theory is shown by the dashed (blue) line, and the open (green) circle with a vertical bar is the $t \to 0$ extrapolation of Fig. 1. A fixed-node Monte Carlo calculation [18] coincides with the solid black line. Inset: Rratio of the condensation energy $\xi_N - \xi_S$ to $\frac{5}{8}(\frac{\Delta}{E_F})^2$.

Strictly speaking, this formula is valid only in the weakly attractive limit $\Delta \to 0$. For an arbitrary interaction, the condensation energy is given by a more involved function of the gap, and based on dimensional arguments, it should be written as

$$\xi_N - \xi_S = \frac{5}{8}\left(\frac{\Delta}{E_F}\right)^2 F(\Delta/E_F), \tag{9}$$

where F is a (yet) unknown function with $F(0) = 1$ to satisfy the BCS prediction. In the spirit of Landau's theory, the $U(1)$ invariance suggests that F can be expanded with $(\Delta/E_F)^2$ instead of k_Fa, and as such, the first beyond-BCS correction should be proportional to $|\Delta/E_F|^2$. At unitarity, where $\Delta \simeq 0.5E_F$ [19], this leads to a moderate 25% correction to the BCS prediction, which suggests that the range of validity of Eq. (8) should extend beyond the strict weakly interacting limit [21].

In order to test the BCS expression, (8), in the BEC-BCS crossover, we compare our measurement of the condensation energy to $\frac{5}{8}(\frac{\Delta}{E_F})^2$ using the values of Δ measured by radio-frequency spectroscopy in [28] [filled (red) circles in Fig. 4. The agreement shown in Fig. 4 indicates that, even in the strongly interacting regime, the BCS expression is remarkably valid. A more stringent test is provided by plotting the ratio between the left-hand and the right-hand sides of Eq. (8) (inset in Fig. 4), and we indeed find a ratio close to unity. Note that calculating this ratio using BCS mean-field theory provides a reasonable estimate [dashed (blue) line in Fig. 4 inset], even though the absolute values of the condensation energy [dashed (blue) line in Fig. 4] or of the pairing gap are both quantitatively inaccurate in the strongly interacting regime.

V. CONCLUSION

In summary, we have measured the condensation energy of a two-component Fermi gas with tunable interactions. The temperature and spin-polarizing field dependence of the normal phase pressure are in good agreement with a Fermi-liquid description. A simple ladder approximation calculation quantitatively reproduces experimental data at zero temperature in the normal phase. Future work will explore the critical region and search for exotic phases such as the FFLO phase [22].

ACKNOWLEDGMENTS

We thank M. Ku and M. Zwierlein for providing their experimental data and F. Werner for the bold diagrammatic Monte Carlo calculations. We acknowledge support from Institut de France (Louis D.), Région Ile de France (IFRAF-C'nano), ERC Ferlodim, and Institut Universitaire de France.

APPENDIX A: CALCULATION OF THE MINORITY DENSITY

Another way to calculate the minority density n_2 is to integrate on the frequency and wave vector the one-particle Green's function,

$$n_{\mathbf{k},2} = \int_{i\mathbb{R}} \frac{d\omega}{2\pi i} e^{\omega\delta} \frac{1}{\left[\omega + \mu_2 - \frac{k^2}{2m} - \Sigma_2(k,\omega)\right]}, \tag{A1}$$

$$n_2 = \frac{1}{2\pi^2}\int_0^{+\infty} k^2 dk\, n_{\mathbf{k},2}, \tag{A2}$$

where $n_{\mathbf{k},2}$ is the occupation number of minority fermions at wave vector $\mathbf{k}$, $\delta \to 0^+$, and we have used the isotropy of $n_{\mathbf{k},2}$. In practice, in order to have a more rapidly converging integral, we add and subtract the free particle Green's function, and we calculate analytically the free particle occupation number. This method is of course much more lengthy than the Landau method, since one has to perform two additional integrations. In the case of a negative chemical potential of the minority particles $\mu_2 < 0$, we find that the Green's function has, for $\mathrm{Re}(\omega) < 0$, a single quasiparticle pole at an energy $E_k < 0$ with a residue Z_k. Therefore we find $n_{\mathbf{k},2} = Z_k$ for $E_k < 0$ or, equivalently, $k < k_{F,2}$ and $n_{\mathbf{k},2} = 0$ for $k > k_{F,2}$. This transforms the integration on frequency into finding a root E_k and computing $Z_k = [1 - \partial\Sigma_2(k,\omega = E_k)/\partial\omega]^{-1}$, which is easier numerically.

Furthermore, we find that for $\mu_2 < 0$, $\Sigma_2(k,\omega;\mu_1, \mu_2,a^{-1}) = F(k,\omega + \mu_2;\mu_1,a^{-1})$. This can be shown by studying the location of the singularities of $\Gamma(K,\Omega)$ in the complex Ω plane and by deforming the integration contour in Eq.(4). As a consequence, the residue Z_k does not depend on μ_2. This simplifies the calculation of the pressure in Eq. (7). Indeed we find

$$\begin{aligned} P(\mu_1,\mu_2;a^{-1}) - P_0(\mu_1) &= \int_{\mu_P}^{\mu_2} d\mu_2'\, n_2(\mu_1,\mu_2';a^{-1}) \\ &= \int_{\mu_P}^{\mu_2} d\mu_2' \int_0^{k_{F,2}(\mu_2')} \frac{dk}{2\pi^2}\, k^2 Z_k \\ &= \int_0^{k_{F,2}(\mu_2)} \frac{dk}{2\pi^2} k^2 Z_k\,(\mu_2 - \mu_F(k))\,, \end{aligned}$$

where we have permuted the integration order between the second and the third lines. We have defined $\mu_F(k)$ such that $\mu_F(k) = k^2/(2m) + \Sigma_2(k,\omega = 0;\mu_1,\mu_2 = \mu_F(k))$ (μ_F is basically the inverse function of $k_{F,2}$). We are left with a single integral and numerical calculation of μ_F and Z_k. The quantities μ_P (polaron chemical potential), $n_2(\mu_2')$ (minority density), $k_{F,2}(\mu_2')$ (minority Fermi wave vector), and Z_k (quasiparticle residue) depend on the majority chemical potential μ_1 and the inverse scattering length a^{-1}.

For the unitary limit, we show in Fig. 5 the results for the reduced EoS $h(b)$ using the two methods [Landau and Eqs. (A1) and (A2)]. We see that the difference between the two methods is small. Due to its simplicity, we therefore use the Landau method.

APPENDIX B: SCATTERING LENGTH CORRECTION OF THE EQUATION OF STATE

While the original data were taken at a magnetic field of 834 G, corresponding to a previous determination of the position of the wide Feshbach resonance between the two lowest energy states of ^{6}Li [29], a more refined measurement involving radio-frequency spectroscopy of a few molecules led to a small downshift of the resonance position, to $B_0 = 832.18(8)$ [10]. The influence of this scattering length change on the thermodynamics can be estimated using the Tan contact $\mathcal{I}$, since it verifies the following relation (the so-called

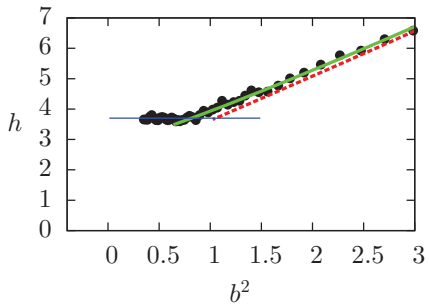

FIG. 5. (Color online) Dimensionless pressure of the spin-imbalanced gas in the unitary limit ($\delta = 0$). Experimental results are shown as filled black circles. The theory using Eq. (6) (Landau's method) is shown by the thick solid (green) line, while the result of Eqs. (A1) and (A2) is shown as the dashed (red) line. The horizontal (blue) line shows the value of the dimensionless pressure in the superfluid state.

adiabatic sweep theorem):

$$\frac{dE}{d(-1/a)} = \frac{\hbar^2}{4\pi m}\mathcal{I}. \tag{B1}$$

The contact can be expressed in the grand-canonical ensemble using the relation

$$\left(\frac{\partial E}{\partial(-1/a)}\right)_{S,V,N} = \left(\frac{\partial\Omega}{\partial(-1/a)}\right)_{T,V,\mu}, \tag{B2}$$

where $\Omega = -PV$ is the grand potential. Using the contact density $C = \mathcal{I}/V$, we can write to lowest order in a^{-1},

$$P(\mu,T,a^{-1}) = P(\mu,T,0) + a^{-1}\frac{\hbar^2}{4\pi m}C(\mu,T,0), \tag{B3}$$

where the contact density at unitarity is a function of $\beta\mu$ only. We can thus write the finite a correction to the dimensionless

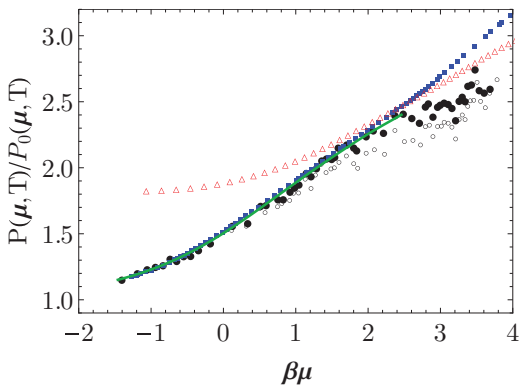

FIG. 6. (Color online) Pressure of the unpolarized unitary Fermi gas. The original data taken at 834 G are shown as open black circles [13], while the corrected EoS at 832.18 G is displayed as filled black circles (see text). Measurements from MIT and Tokyo are shown as filled (blue) squares [15] and open (red) triangles [31], respectively, and the bDMC calculation from Amherst, as the solid (green) line [16]. At the lowest temperatures, we find a corrected Bertsch parameter, $\xi_S = 0.40(2)$.

pressure,

$$\frac{P(\mu,T)}{P_0(\mu,T)} = \frac{P(\mu,T,a^{-1})}{P_0(\mu,T)} + \frac{1}{8\pi^2}\frac{\lambda_{\mathrm{dB}}}{a}\frac{\tilde{C}(\beta\mu)}{\mathrm{Li}_{5/2}(-\exp(\beta\mu))}, \tag{B4}$$

where $P_0(\mu,T)$ is the pressure of the noninteracting Fermi gas, and $\tilde{C}(\beta\mu) = C\lambda_{\mathrm{dB}}^4$ is the dimensionless contact density. $\tilde{C}(\beta\mu)$ has recently been calculated by the diagrammatic Monte Carlo method [30]. We compute the small a correction by applying Eq. (B4) to the pressure extracted from each ^{6}Li density profile used in the measurement of the EoS. The temperature in Eq. (B4) is determined from the ^{7}Li thermometer, and the full EoS is reconstructed by first adjusting μ_0 for each high-temperature image to match the virial expansion and then progressively connecting lower temperature images to high-$\beta\mu$ ones, as originally done in [13]. The result for the pressure is shown in Fig. 6.

[1] J. Schrieffer, *Theory Of Superconductivity* (Perseus Books, New York, 1999).
[2] A. Leggett, Science **274**, 587 (1996).
[3] E. Demler and S. Zhang, Nature **396**, 733 (1998).
[4] D. J. Scalapino and S. R. White, Phys. Rev. B **58**, 8222 (1998).
[5] R. Haslinger and A. V. Chubukov, Phys. Rev. B **68**, 214508 (2003).
[6] S. Chakravarty, H.-Y. Kee, and E. Abrahams, Phys. Rev. B **67**, 100504(R) (2003).
[7] D. Van der Marel, A. J. Leggett, J. W. Loram, and J. R. Kirtley, Phys. Rev. B **66**, 140501(R) (2002).
[8] S. Chakravarty, H.-Y. Kee, and E. Abrahams, Phys. Rev. Lett. **82**, 2366 (1999).
[9] I. Bloch, J. Dalibard, and W. Zwerger, Rev. Mod. Phys. **80**, 885 (2008).
[10] G. Zürn, T. Lompe, A. N. Wenz, S. Jochim, P. S. Julienne, and J. M. Hutson, Phys. Rev. Lett. **110**, 135301 (2013).
[11] C.-H. Cheng and S.-K. Yip, Phys. Rev. B **75**, 014526 (2007).
[12] T. Ho and Q. Zhou, Nat. Phys. **6**, 131 (2009).
[13] S. Nascimbène, N. Navon, K. Jiang, F. Chevy, and C. Salomon, Nature **463**, 1057 (2010).
[14] N. Navon, S. Nascimbène, F. Chevy, and C. Salomon, Science **328**, 729 (2010).
[15] M. Ku, A. Sommer, L. Cheuk, and M. Zwierlein, Science **335**, 563 (2012).
[16] K. Van Houcke, F. Werner, E. Kozik, N. Prokofev, B. Svistunov, M. Ku, A. Sommer, L. Cheuk, A. Schirotzek, and M. Zwierlein, Nat. Phys. **8**, 366 (2012).
[17] S. Nascimbène, N. Navon, F. Chevy, and C. Salomon, New J. Phys. **12**, 103026 (2010).
[18] S. Nascimbène, N. Navon, S. Pilati, F. Chevy, S. Giorgini, A. Georges, and C. Salomon, Phys. Rev. Lett. **106**, 215303 (2011).
[19] J. Carlson, S.-Y. Chang, V. R. Pandharipande, and K. E. Schmidt, Phys. Rev. Lett. **91**, 050401 (2003).
[20] C. Lobo, A. Recati, S. Giorgini, and S. Stringari, Phys. Rev. Lett. **97**, 200403 (2006).
[21] A. Bulgac, J. E. Drut, and P. Magierski, Phys. Rev. A **78**, 023625 (2008).
[22] Edited by W. Zwerger, *The BEC-BCS Crossover and the Unitary Fermi Gas, Lecture Notes in Physics, Vol. 836* (Springer, Berlin, 2012).
[23] P. Pieri and G. C. Strinati, Phys. Rev. B **61**, 15370 (2000); A. Perali, P. Pieri, G. C. Strinati, and C. Castellani, *ibid.* **66**, 024510 (2002); A. Perali, P. Pieri, and G. C. Strinati, Phys. Rev. Lett. **93**, 100404 (2004); P. Perali, P. Pieri, L. Pisani, and G. C. Strinati, *ibid.* **92**, 220404 (2004).
[24] R. Combescot, X. Leyronas, and M. Yu. Kagan, Phys. Rev. A **73**, 023618 (2006).
[25] R. Combescot, A. Recati, C. Lobo, and F. Chevy, Phys. Rev. Lett. **98**, 180402 (2007).
[26] F. Chevy, Phys. Rev. A **74**, 063628 (2006); N. V. Prokof'ev and B. V. Svistunov, Phys. Rev. B **77**, 020408 (2008); R. Combescot and S. Giraud, Phys. Rev. Lett. **101**, 050404 (2008); R. Combescot, S. Giraud, and X. Leyronas, Europhys. Lett. **88**, 60007 (2009).
[27] The correspondence formulas from the canonical to the grand-canonical ensemble can be found in the Supplementary Material to [14]. Since the formulas involve derivatives, it is convenient to parametrize the data points with rational functions (solid lines in Fig. 3).
[28] A. Schirotzek, Y.-il Shin, C. H. Schunck, and W. Ketterle, Phys. Rev. Lett. **101**, 140403 (2008).
[29] M. Bartenstein, A. Altmeyer, S. Riedl, R. Geursen, S. Jochim, C. Chin, J. H. Denschlag, R. Grimm, A. Simoni, E. Tiesinga, C. J. Williams, and P. S. Julienne, Phys. Rev. Lett. **94**, 103201 (2005).
[30] K. Van Houcke, F. Werner, E. Kozik, N. Prokof'ev, and B. Svistunov, arXiv:1303.6245.
[31] M. Horikoshi, S. Nakajima, M. Ueda, and T. Mukaiyama, Science **327**, 442 (2010).